

# Interannual covariability in remotely sensed vegetation index and actual evapotranspiration over northern Eurasia

Rikie Suzuki, Kooiti Masuda, and Dennis Dye

Frontier Research Center for Global Change, Japan Agency for Marine-Earth Science and Technology,  
Yokohama 236-0001, Japan – (rikie, masuda, dye)@jamstec.go.jp

**Abstract** – The covariability between the interannual changes of Normalized Difference Vegetation Index (NDVI) and actual evapotranspiration was examined. This study employed NDVI datasets from the Pathfinder AVHRR Land (PAL) data and the Global Inventory Monitoring and Modeling Studies (GIMMS) group to reduce the uncertainty that may be involved in the NDVI time series. The analysis was carried out for the northern Asia region from 1982 to 2000. 19-year interannual change in PAL-NDVI and GIMMS-NDVI were both compared with interannual change in actual ET which was estimated from model-assimilated atmospheric data and gridded precipitation data. For both NDVI datasets the annual maximum correlation with ET occurs in June, which is near the central period of the growing season. A significant positive correlation between NDVI and ET interannual changes was observed over most of the vegetated land area in June in PAL and GIMMS-NDVIs. These results suggest that the control of interannual change in ET is dominated by interannual change in vegetation activity. Based on analyses of temperature, precipitation, and NDVI interannual changes, it was found that the study area is roughly divided into two regions: the warmth dominant northmost region and the wetness dominant southern region. These results indicate that the vegetation interannual change and the resultant ET interannual change are controlled by warmth and wetness in these two regions, respectively.

**Keywords:** Siberia, Taiga, climate system, phenology

## 1. INTRODUCTION

Vegetation over an extensive area influences actual evapotranspiration (ET) from the land to the atmosphere mainly through transpiration activity. The authors' previous study, Suzuki and Masuda (2004), found an interannual covariability between ET and the Normalized Difference Vegetation Index (NDVI), a remotely-sensed measure of vegetation greenness, over a continental-scale land surface. This result suggested that vegetation is a major factor controlling interannual variation in ET, and therefore vegetation change must be considered to predict future changes in ET and climate. In this prior study, NDVI data from the Pathfinder AVHRR Land (PAL) dataset were analyzed. However, studies of NDVI interannual change are subject to uncertainty, because NDVI data often contain errors associated with sensor- and atmosphere-related effects. This study aimed to reduce this uncertainty by employing a second major NDVI dataset, from the Global Inventory Monitoring and Modeling Studies (GIMMS) group, in addition to PAL. GIMMS-NDVI data were produced with a calibration method that differs from the one employed for PAL-NDVI data. An intercomparison of the PAL-NDVI and GIMMS-NDVI datasets provide an effective basis for further analysis of the covariability of NDVI and ET interannual changes. Furthermore,

this study made an attempt to elucidate the cause of the interannual changes in NDVI and ET in relation to temperature and precipitation interannual changes.

## 2. DATA AND METHOD

The NDVI is defined as  $NDVI = (Ch2 - Ch1)/(Ch2 + Ch1)$ , where  $Ch1$  and  $Ch2$  are measurements from Advanced Very High Resolution Radiometer (AVHRR) channels 1 (visible) and 2 (near-infrared) of NOAA satellite, respectively. Analyses were conducted on the monthly basis from 1982 to 2000 over northern Asia (30°E – 150°E, 30°N – 75°N).

### 2.1 PAL NDVI

The NDVI value from 10-daily PAL dataset (1 x 1-degree spatial resolution) was examined. The monthly value was composited by choosing the highest NDVI among three 10-day datasets for each month. This process effectively removed cloud-contaminated observations. The 1 x 1-degree value was resampled into 2.5 x 2.5-degree grid system to link with the ET grid system.

The PAL data are adjusted for errors caused by non-vegetative factors such as satellite orbit drift, sensor degradation, and ozone concentration and represent interannual variation in vegetation well. Atmospheric Rayleigh scattering and ozone absorption were corrected. Scan angle criteria is within +/- 42 degrees of nadir. The influence due to sensor degradation and orbital drift were adjusted according to the empirical formula (Rao and Chen, 1995, 1996). Intercalibration with NOAA-9 and other NOAA was also conducted.

### 2.2 GIMMS NDVI

The NDVI value from 15-daily GIMMS dataset (8 x 8 km spatial resolution) (Pinzon et al., 2004; Pinzon, 2002; Tucker et al., 2005) was compared with PAL-NDVI. First, the original 8 km pixel value was resampled into 1 x 1-degree grid system. Then, monthly data were composited by choosing the higher NDVI between two 15-daily datasets for each month. The 1 x 1-degree value was resampled into 2.5 x 2.5-degree grid system as well as PAL-NDVI.

The GIMMS data are also adjusted for non-vegetative factors and represent interannual variation in vegetation well. The effects by stratospheric aerosol due to El Chichon and Mt. Pinatubo volcanic eruptions were adjusted. No correction for stratospheric ozone, Rayleigh scattering, and water vapor was considered. Cloud was screened according to 273°K of the brightness temperature of  $Ch5$ . Scan angle criteria is within +/- 40 degrees of nadir. Calibration for sensor degradation was executed based on an algorithm different from PAL (Vermote and Kaufman, 1995; Los, 1998), and the desert correction. For the calibration of the orbital drift, Pinzon's (Pinzon, 2002) scheme was applied.

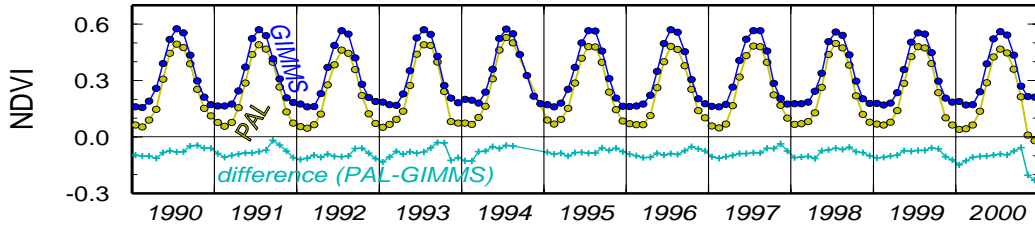


Fig. 1. Mean temporal change of PAL-NDVI (yellow), GIMMS-NDVI (blue), and their difference (PAL – GIMMS) (light blue) from 1990 to 2000 (30°E – 150°E, 30°N – 75°N).

Intercalibration with MODIS and SPOT-4/ VEGETATION was also conducted.

### 2.3 Evapotranspiration

ET from the land surface can be estimated from the atmospheric water budget (Peixoto and Oort, 1992). ET from the bottom (i.e., land surface) of an air column, which vertically extends from the ground surface to the top of the atmosphere, can be expressed by the following atmospheric water budget equation:

$$ET = P + \frac{\partial W}{\partial t} + \nabla_H \cdot \bar{Q}$$

where  $t$  is the time,  $P$  is the precipitation at the bottom,  $W$  is the precipitable water in the air column, and  $\nabla_H \cdot \bar{Q}$  is the horizontal flux divergence of water vapor integrated from the surface to the top of the atmosphere (so called aerial runoff).

This study assumed air columns above the 2.5 x 2.5-degree grid cells and computed each term for each grid cell. The CPC Merged Analysis of Precipitation (CMAP) dataset was used to determine monthly precipitation  $P$  (Xie and Arkin, 1997). The terms  $\nabla_H \cdot \bar{Q}$  and  $\partial W/\partial t$  are computed from specific humidity and wind values. In the present study, these meteorological values were obtained from gridded 6-hourly atmospheric data (NCEP Reanalysis-2) provided by the National Centers for Environmental Prediction (NCEP) (Kanamitsu et al., 2002).

Monthly  $\nabla_H \cdot \bar{Q}$  from 1982 to 2000 for each grid cell (192 x 94) of the reanalysis model was estimated by integrating the flux divergence from the ground to 0 hPa (all 28 layers of the model). The estimated values were interpolated onto the same 2.5 x 2.5-degree grid as the CMAP data. The monthly  $\partial W/\partial t$  was calculated from the precipitable water difference between the beginning and end of each month.

### 2.4 Temperature

Additionally, gridded surface temperature data were obtained from the CRU TS 2.0 dataset, which is comprised of monthly grids of observed climate data. The dataset spans the period from 1901 to 2000 and covers the global land surface at 0.5-degree resolution ([http://www.cru.uea.ac.uk/~timm/grid/CRU\\_TS\\_2\\_0.html](http://www.cru.uea.ac.uk/~timm/grid/CRU_TS_2_0.html)).

Some dataset values were not suitable for long-term variation analysis, because interpolation and substitution of values occurred frequently in regions with sparse station networks, especially in the early years of the period. However, we regarded the temperature time series over northern Asia from 1982 to 2000 as representative for interannual temperature variation analysis,

since northern Asia had a sufficiently dense surface station network during that period.

## 3. RESULT AND DISCUSSION

### 3.1. Comparison of Temporal Variation

Fig. 1 demonstrates the time series of mean PAL-NDVI, GIMMS-NDVI and their difference from 1990 to 2000 averaged over the study region. These variations are similar. Both NDVIs indicate striking seasonal change, that is, small value in winter and high value in summer, reflecting the vegetation phenology in the region. However GIMMS-NDVI indicates higher value than that of PAL-NDVI throughout the year as known from the negative difference (PAL – GIMMS) value in Fig. 1. Their difference tends to be small in autumn which is related to the larger PAL-NDVI than GIMMS-NDVI in October over boreal forest zone.

### 3.2. Interannual Changes of NDVIs and ET

Fig. 2 shows the correlation coefficients between 19-year interannual changes of PAL-NDVI and ET anomalies, and GIMMS-NDVI and ET anomalies for each month averaged over three representative regions (see the caption of Fig. 2 for three regions). Annually, the highest correlation was found in June in all three regions in both cases of PAL and GIMMS. For example, western Siberia has the highest coefficient (0.73) for PAL-NDVI in June, while the highest coefficient of GIMMS-NDVI is found

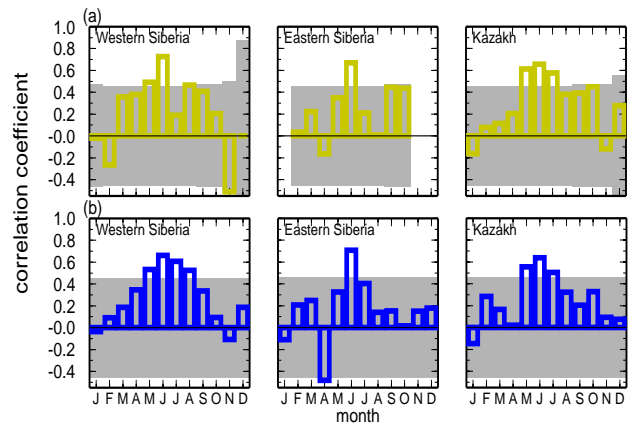


Fig. 2 Monthly Correlation coefficients of the PAL-NDVI and ET (a), GIMMS-NDVI and ET (b) interannual changes from 1982 to 2000 for the three study regions; Western Siberia (50°E – 90°E, 55°N – 65°N), Eastern Siberia (80°E – 130°E, 65°N – 70°N), and Kazakh (50°E – 60°E, 45°N – 55°N). The gray area denotes values below the 99% significance level.

in Eastern Siberia (0.71) in June. Since June is the most active season of vegetation, the highest correlation between NDVIs and ET is attributed to the greatest contribution of the vegetation transpiration to total ET in June. The fact that the highest correlation coefficient occurs in June in both cases of PAL-NDVI and GIMMS-NDVI surely delineates the close interannual relationship between vegetation and ET.

19-year interannual changes (monthly anomalies) in the PAL-NDVI, GIMMS-NDVI, and ET in June, the month with the highest coefficient, over the three regions were indicated in Fig. 3. Very similar interannual changes among three parameters can be seen in each region. This result indicates that both PAL-NDVI and GIMMS-NDVI display interannual variation that is similar to ET for active growing season months.

### 3.3. NDVI Correlation to Temperature and Precipitation Interannual Changes

To investigate the cause of NDVI and ET interannual changes, the interannual correlation coefficient between temperature (from CRU TS2.0 dataset) and NDVI, and precipitation (from CMAP dataset) and NDVI was calculated. Fig. 4 demonstrates those relationships for PAL-NDVI and GIMMS-NDVI in June, when the correlation between NDVI and ET is the strongest in the year. Each plotted point in Fig. 4 corresponds to those correlation values in each 2.5 x 2.5 degree grid cell over the study region.

In both cases, most of points are plotted in the lower-right, upper-right, and upper-left quadrants of the coordinate system, and few points in lower-left quadrant. The points plotted in the lower-right quadrant indicate that the NDVI interannual change is positively dominated by temperature and negatively by precipitation, suggesting the vegetation interannual change is dominated by warmth interannual change. On the other hand, those in the upper-left quadrant indicate that the NDVI interannual change is positively dominated by precipitation and negatively by temperature, suggesting that the vegetation interannual change is dominated by wetness interannual change. Those in upper-right quadrant mean that both temperature and precipitation positively control the NDVI interannual change,

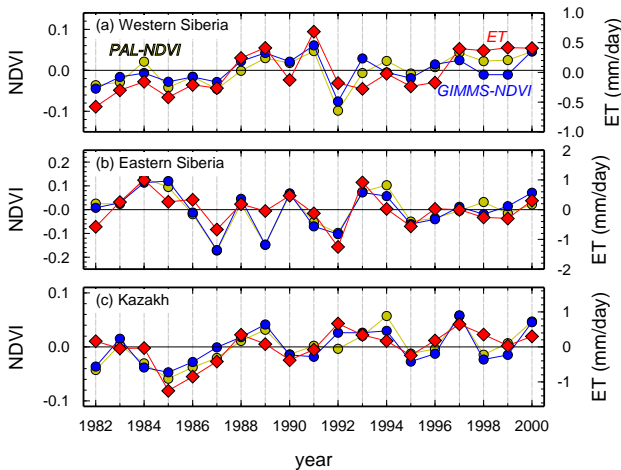


Fig. 3. Interannual variation of the PAL-NDVI (yellow), GIMMS-NDVI (blue) and ET (red) anomalies averaged in June in the three selected regions. (see the caption of Fig. 2 for the longitude and latitude for these three regions).

suggesting the vegetation is positively dominated by both warmth and wetness interannual changes. In all the quadrants, most of the correlation coefficient between NDVI and ET shows positive value, delineating that NDVI positively influence ET interannual change in any cases.

Fig. 5 illustrates the geographical distribution of correlation coefficients between temperature and NDVI interannual changes, and between precipitation and NDVI interannual changes in June for PAL-NDVI and GIMMS-NDVI. In both PAL-NDVI and GIMMS-NDVI panels, red color (positive temperature-NDVI and negative precipitation-NDVI correlations) distributes over the northern area, while blue color (negative temperature-NDVI and positive precipitation-NDVI correlations) distributes over the southern part. The green color (positive temperature-NDVI and positive precipitation-NDVI correlations) can be seen at the boundary between red and blue color areas which are roughly

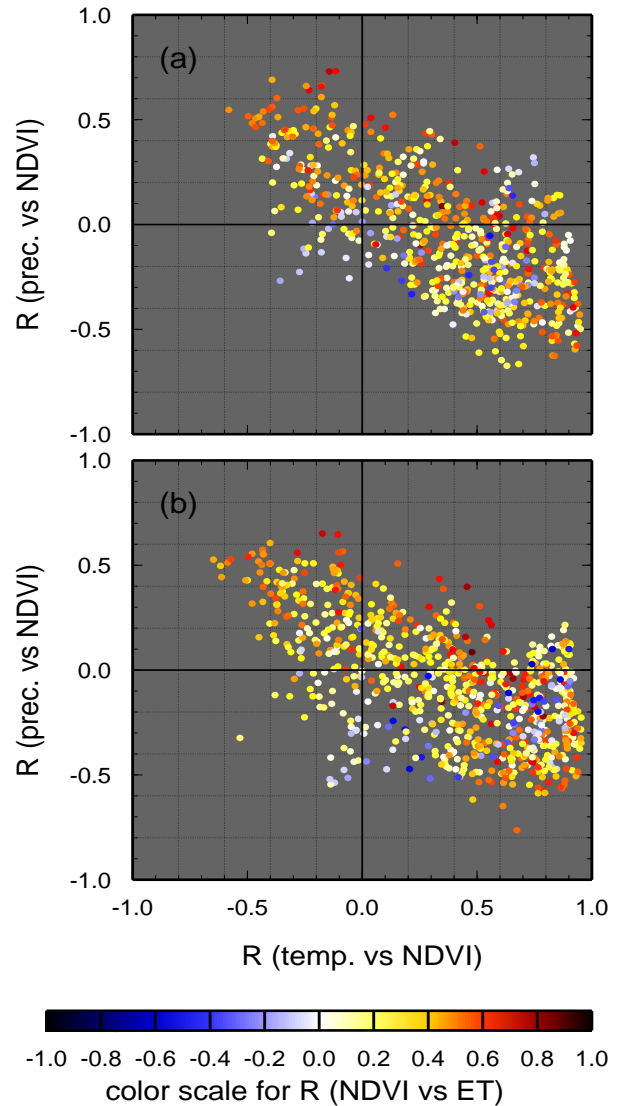


Fig. 4. The relationship between correlation coefficients: temperature and NDVI, and precipitation and NDVI interannual changes for PAL-NDVI (a) and GIMMS-NDVI (b) in June. The correlation coefficient between NDVI and ET was denoted by color scale.

positioned along 55°N latitude.

Figs. 4 and 5 suggest that the vegetation interannual change is induced by warmth interannual change in northern part, while by wetness interannual change in southern part. Subsequently, such vegetation interannual change positively induces the ET interannual change over the area.

#### 4. CONCLUSION

PAL-NDVI and GIMMS-NDVI were both compared with interannual change in ET, which was estimated by model-assimilated atmospheric data and precipitation data. Although the correlation coefficient between GIMMS-NDVI and ET is slightly less than for PAL-NDVI and ET, for both NDVI datasets the annual maximum correlation with ET occurs in June, which is near the central period of the growing season. A positive correlation between GIMMS-NDVI and ET was observed over most of the vegetated land area in June, and a similar result was obtained with PAL-NDVI. The regionality of the interannual correlation between temperature and NDVI, and precipitation and NDVI suggest that the NDVI interannual change, and ET interannual change, which includes the influence of vegetation interannual change, is induced by warmth interannual change in the northern area, and by wetness interannual change in the southern part.

#### 5. REFERENCES

M. Kanamitsu, W. Ebisuzaki, J. Woollen, S.-K. Yang, J.J. Hnilo, M. Fiorino, and G.L. Potter, "NCEP/DOE AMIP-II Reanalysis (R-2)," *Bull. Amer. Meteor. Soc.*, vol 83, p.p. 1631 – 1643, 2002.

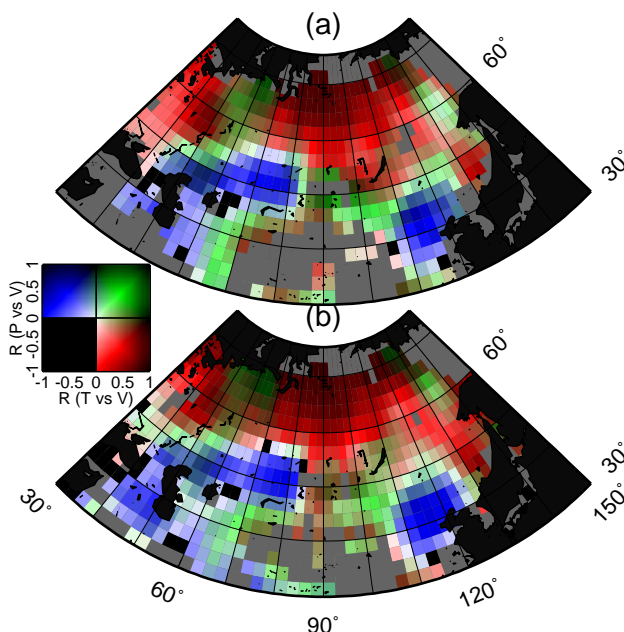


Fig. 5 distribution of the combination of correlation coefficients: temperature and NDVI interannual changes, and precipitation and NDVI interannual changes for PAL-NDVI (a) and GIMMS-NDVI (b) in June. Gray area denotes the NDVI is too small for the calculation of the coefficient.

S.O. Los, "Estimation of the ratio of sensor degradation between NOAA AVHRR channels 1 and 2 from monthly NDVI composites," *IEEE Trans. Geosci. Remote Sensing*, vol 36, p.p. 206 – 213, 1998.

J.P. Peixoto and A.H. Oort, "Physics of Climate," American Institute of Physics, NY, 1992.

J. Pinzon, M.E. Brown, and C.J. Tucker, "Satellite time series correction of orbital drift artifacts using empirical mode decomposition." In *Hilbert-Huang Transform: Introduction and Applications*, N. Huang (eds.), Chapter 10, Part II. Applications (to appear) 2004.

J. Pinzon, "Using HHT to successfully uncouple seasonal and interannual components in remotely sensed data," *Proc. SCI 2002*. Jul 14 – 18, Orlando, Florida, 2002.

C.R.N. Rao, and J. Chen, "Inter-satellite calibration linkages for the visible and nearinfrared channels of the Advanced Very High Resolution Radiometer on the NOAA-7, -9, and -11 spacecraft," *Int. J. Remote Sensing*, vol 16, p.p. 1931 – 1942, 1995.

C.R.N. Rao, and J. Chen, "Post-launch calibration of the visible and near-infrared channels of the advanced very high resolution radiometer on the NOAA-14 space-craft," *Int. J. Remote Sensing*, vol 17, p.p. 2743 – 2747, 1996.

R. Suzuki and K. Masuda, "Interannual covariability found in evapotranspiration and satellite-derived vegetation indices over northern Asia," *J. Meteor. Soc. Japan*, vol 82, p.p. 1233 – 1241, 2004.

C.J. Tucker, J.E. Pinzon, M.E. Brown, D. Slayback, E.W. Pak, R. Mahoney, E. Vermote, and N. El Saleous, "An extended AVHRR 8-km NDVI data set compatible with MODIS and SPOT vegetation NDVI data," *Int. J. Remote Sensing* (submitted), 2005.

E. Vermote and Y.J. Kaufman, "Absolute calibration of AVHRR visible and nearinfrared channels using ocean and cloud views," *Int. J. Remote Sensing*, vol 16, p.p. 2317 – 2340, 1995.

P. Xie and P.A. Arkin, "Global precipitation: A 17-year monthly analysis based on gauge observations, satellite estimates, and numerical model outputs," *Bull. Amer. Meteor. Soc.*, vol 78, p.p. 2539 – 2558, 1997.